Impact of diffusive motion on anomalous dispersion in structured disordered media: From correlated Lévy flights to continuous time random walks

Alessandro Comolli[1,2,3,*] and Marco Dentz[1,3]

[1]*Spanish National Research Council (IDAEA-CSIC), 08034 Barcelona, Spain*

[2]*Department of Civil and Environmental Engineering, Technical University of Catalonia (UPC), 08034 Barcelona, Spain*

[3]*Associated Unit: Hydrogeology Group (UPC-CSIC), 08034 Barcelona, Spain*

(Received 20 February 2018; published 31 May 2018)

We elucidate the impact of diffusive motion on the nature of anomalous dispersion in layered and fibrous disordered media. We consider two types of disorder characterized by quenched random velocities and quenched random retardation properties. Purely advective particle motion is ballistic in both disorder models. This changes dramatically in the presence of transverse diffusion, which leads to dimension-dependent disorder sampling. For $d \leqslant 3$ dimensions, heavy-tailed velocity distributions render large-scale particle motion a correlated Lévy flight, while transport in the quenched random retardation model behaves as a biased continuous time random walk with correlated time increments.

DOI: 10.1103/PhysRevE.97.052146

I. INTRODUCTION

Anomalous dispersion can be seen as the result of the interaction of microscopic advective-diffusive mass transfer and spatial disorder, which may hinder or facilitate transport. Subdiffusive transport may be induced by crowdedness, randomly distributed traps, and retardation properties, which quantify physical and chemical interactions between the transported substance and the medium. Superdiffusion, on the other hand, may be induced by strong disorder correlation [1–4]. Anomalous dispersion as manifested, for example, in heavy-tailed first-passage time distributions, and nonlinear evolution of particle displacement variance has been ubiquitously observed across spatial and temporal scales ranging from natural and engineered porous media [5–13], biological tissue [14–17], optical media [18,19], turbulence [20], and other physical systems [21]. Anomalous dispersive behaviors in disordered media have been modeled using stochastic approaches such as Lévy flights [22,23], Lévy walks [24], continuous time random walk (CTRW) [1,4,10,25,26], fractional Brownian motion and generalized Langevin equations [27–29], and Brownian motion with nonstationary increments [30].

Key questions we address in this paper refer to the origins of anomalous dispersion in terms of medium geometry, disorder properties, and microscopic mass transfer mechanisms. The latter play a pivotal role for the way disorder is sampled, which determines the large-scale particle motion and its ergodic and self-averaging properties. For diffusive motion in unstructured disordered media characterized by independent quenched random traps, for example, the nature of the (CTRW-type) average particle motion and self-averaging properties of subdiffusion depend on the dimensionality of space [1,17,31–34] as a consequence of the diffusive disorder sampling. For biased, purely advective particle motion in unstructured media with random retardation or random conductivity, large-scale transport follows (coupled) CTRW dynamics [3,7,11,35–39]. Advective-diffusive transport in stratified media, on the other hand, leads to average particle dynamics that can be described as a fractional Brownian motion [6,40–42], while purely advective motion in such media is the prototype of ballistic dispersion.

In this paper, we study the impact of diffusion on advective transport in structured disordered media. We consider media organized in channels ($d \geqslant 3$ dimensions) or strata ($d = 2$ dimensions) as illustrated in Fig. 1. This type of stratified or fibrous medium geometries can be found in geological media (e.g., sedimentary formations), engineered materials (e.g., capillary bundles, filters), and biological media (e.g., neuronal fiber pathways). We consider advection-driven microscopic transport of a scalar $c(\mathbf{x},t)$ given by the Fokker-Planck equation

$$\frac{\partial c(\mathbf{x},t)}{\partial t} + u(\mathbf{z})\frac{\partial c(\mathbf{x},t)}{\partial x} - \nabla_z^2 \mathcal{D}(\mathbf{z}) c(\mathbf{x},t) = 0, \tag{1}$$

where $u(\mathbf{z})$ and $\mathcal{D}(\mathbf{z})$ are drift and diffusion coefficients that vary randomly between the channels or strata. The coordinate vector is denoted by $\mathbf{x} = (x,\mathbf{z})^\top$ with $\mathbf{z} = (z_2,\ldots,z_d)^\top$. Diffusion along the channels is disregarded because it is subleading compared to the disorder impact on longitudinal motion. The Fokker-Planck equation (1) is equivalent to the Langevin equations

$$dx(t) = u[\mathbf{z}(t)]dt, \quad d\mathbf{z}(t) = \sqrt{2Ddt}\boldsymbol{\zeta}(t), \tag{2}$$

where $\boldsymbol{\zeta}(t)$ is a $d_w = (d-1)$-dimensional white noise, which models the transverse diffusive motion between the strata or fibers. Here and throughout the paper the noise average is indicated by angular brackets while disorder-averaged quantities are marked by an overbar. In the absence of transverse diffusion, this means without noise, the trajectory of a particle originating in $\mathbf{z}_0 = \mathbf{z}(t=0)$ is simply $x(t) = u(\mathbf{z}_0)t$. Thus, the ensemble averaged particle density in flow direction is $c(x,t) = \overline{\delta[x - u(\mathbf{z}_0)t]}$, and more explicitly

$$c(x,t) = \frac{1}{t} p_u(x/t), \tag{3}$$

*alessandro.comolli@idaea.csic.es

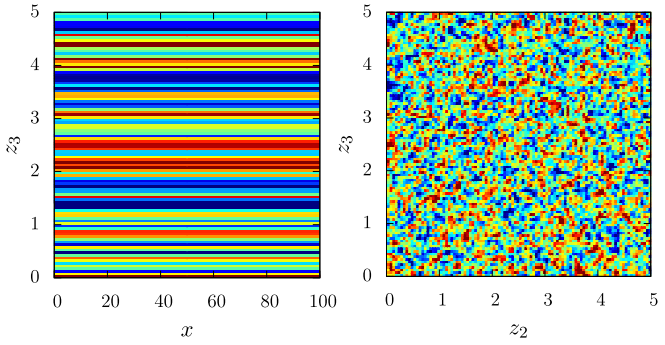

FIG. 1. (Left) Lateral and (right) frontal view of a $d = 3$-dimensional disordered medium composed of channels of equal size ℓ. The colors represent different medium properties.

where $p_u(u)$ is the velocity distribution between the channels or strata. The first-passage time distribution $f(t,x) = \overline{\delta[t - x/u(\mathbf{z}_0)]}$ is

$$f(t,x) = \frac{x}{t^2} p_u(x/t). \tag{4}$$

This type of models, sometimes including longitudinal diffusion, have been known as stochastic convective streamtube models in the literature [43–45]. In this paper we focus on the decisive role of transverse diffusion for large-scale transport.

We first consider the Matheron–de Marsily random velocity model [6], which assigns a random velocity to each layer or channel such that $u(\mathbf{z}) = v(\mathbf{z})$ and $\mathcal{D}(\mathbf{z}) = D$, where D is the diffusion coefficient. For flow in porous media, Darcy's law [46] relates the flow velocity $v(\mathbf{z})$ to hydraulic conductivity $k(\mathbf{z})$. Second, we consider a random retardation model, which accounts for particle retention due to physical or chemical interactions with the medium such as fast linear adsorption reactions. The drift and diffusion coefficients in this model read as $u(\mathbf{z}) = v_0/\theta(\mathbf{z})$ and $\mathcal{D}(\mathbf{z}) = D/\theta(\mathbf{z})$, where v_0 is a constant flow velocity and $\theta(\mathbf{z})$ the random retardation coefficient. In the absence of diffusion, this means for $D = 0$, both disorder models give ballistic motion. Notice that the presence of transverse diffusion has a significant impact on longitudinal transport. Diffusion shortens the velocity correlation length, which would be otherwise infinite. Thus, it enables particles to explore the disorder. The efficiency of transverse diffusion as a sampling mechanism grows with increasing spatial dimension because the return probability to a previously visited channel decreases. In the following, we study these mechanisms and the consequences for average transport in the two disorder models in detail.

II. MATHERON–DE MARSILY MODEL

We start our analysis with the Langevin equation equivalent to (1) for the random velocity model, which reads as

$$dx(t) = v[\mathbf{z}(t)]dt, \quad d\mathbf{z}(t) = \sqrt{2Ddt}\boldsymbol{\zeta}(t). \tag{5}$$

The random velocities $v \geqslant 0$ are distributed between channels according to $p_v(v)$. Note that particle motion in transverse direction describes a $d_w = (d-1)$-dimensional random walk such that $\langle \mathbf{z}(t) \rangle = \mathbf{0}$ and $\langle \mathbf{z}(t)^2 \rangle = 2d_w Dt$.

In order to quantify the average particle motion, we discretize (5) such that $\Delta\mathbf{z}(t)$ is oriented along the coordinate axes and $\|\Delta\mathbf{z}(t)\| = \ell$, which implies that particles change channels at each random walk step. The time required is equal to the first-passage time τ across the distance ℓ by pure diffusion, which is approximated here by an exponential random variable τ with mean $\tau_D = \ell^2/d_w D$ [47,48]. The resulting time-domain random walk is given by

$$x_{n+1} = x_n + v_n\tau_n, \quad t_{n+1} = t_n + \tau_n, \tag{6}$$

where we defined $v_n \equiv v(\mathbf{z}_n)$. In the transverse directions, particles perform a random walk on a d_w-dimensional hyperlattice according to $\mathbf{z}_{n+1} = \mathbf{z}_n + \ell\boldsymbol{\zeta}_n$, where the random vector $\boldsymbol{\zeta}$ has unit length and points into the direction of any of the transverse coordinate axes with equal probability. The numerical simulations reported in the following are based on this time-domain random walk (TDRW) scheme. The TDRW has been used in the literature for the efficient solution of diffusion and advection-diffusion transport problems in heterogeneous porous and fractured media [49–51].

For the derivation of the large-scale transport behaviors, we approximate the transition time τ_n for a single step by its mean τ_D. The space increments $\Delta x = v\tau_D$ in (8) thus are distributed according to

$$\psi_\Delta(x) = \frac{1}{\tau_D} p_v(x/\tau_D). \tag{7}$$

In order to understand the large-scale transport behavior, it is important to note that the series of random velocities v_n and thus space increments Δx_n depends on the transverse random walk process. Thus subsequent v_n are in general not independent because particles may visit the same site repeatedly according to Polya's theorem. This notion is quantified by the average number S_n of distinct sites visited by a random walker on a d_w-dimensional hyperlattice [1,52]. For diffusion in $d_w < 2$ transverse dimensions, S_n increases as the volume swept by an ensemble of random walkers $\sim n^{d_w/2}$; for $d_w = 2$, S_n increases sublinearly as $\sim n/\ln(n)$; and for $d_w > 2$, S_n increases proportional to the number of random walk steps $\sim n$. This means that after n steps a particle has seen in average $\gamma_n = n/S_n$ times the same channel. Thus, the particle trajectory along the channels can be renormalized in terms of independent increments as [1]

$$x_n = \gamma_n \sum_{i=1}^{S_n} v_i \tau_D. \tag{8}$$

This means that the impact of transverse noise on particle motion is accounted for through the random sampling of flow velocities and the renormalization with S_n, see also Ref. [34].

A. Spatial density and moments

The coarse-grained longitudinal particle position at time t is given by $x(t) = x_{n_t}$, where $n_t = t/\tau_D$ denotes the average number of steps needed to reach t by the time process in (6). The average particle distribution is

$$c(x,t) = \overline{\delta(x - x_{n_t})}. \tag{9}$$

In the absence of transverse diffusion, the particle distribution is given by (3), this means it is obtained by a direct map

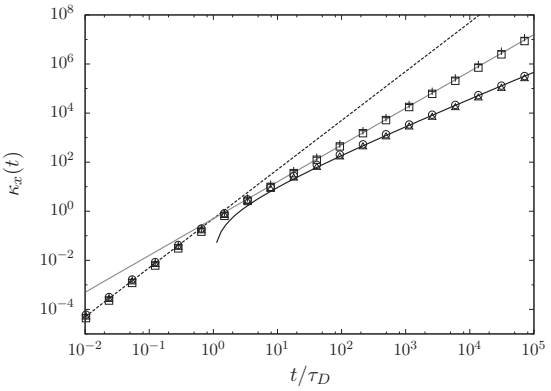

FIG. 2. Displacement variance for $\delta = 1/2$ (crosses for $d = 2$ and circles for $d = 3$) and $\delta = 3/2$ (squares for $d = 2$ and triangles for $d = 3$). The solid lines represent the asymptotic scalings (13), and the dashed line the ballistic behavior.

from the velocity distribution. Here this is different. The particle position (8) is given by the sum of S_n independent increments. Thus, $c(x,t)$ is given by the S_{n_t}-fold convolution of the increment distribution (7). Note that the disorder average in (9) removes the dependence on the noise realizations [34].

In the following, we study the spatial particle distributions and the displacement moments if they exist. Specifically, the mean displacement $\mu_x(t)$ and the displacement variance $\kappa_x(t)$ are defined by

$$\mu_x(t) = \overline{x_{n_t}}, \tag{10a}$$

$$\kappa_x(t) = \overline{[x_{n_t} - \mu_x(t)]^2}. \tag{10b}$$

We first consider the case of velocity distributions characterized by finite velocity variance, then the case of heavy-tailed velocity distributions.

1. Finite velocity variance

For $S_{n_t} \gg 1$, this means for $t \gg \tau_D$, the central limit theorem implies that the particle distribution is given by the Gaussian distribution

$$c(x,t) = \frac{\exp\left[-\frac{(x-\overline{v}t)^2}{2\kappa_x(t)}\right]}{\sqrt{2\pi\kappa_x(t)}}. \tag{11}$$

The displacement variance $\kappa_x(t)$ obtained by using (8) in (10) as

$$\kappa_x(t) = \sigma_v^2\tau_D^2\frac{(t/\tau_D)^2}{S_{n_t}}. \tag{12}$$

Recall that the scaling of the number of distinct visited sites S_n depends on the transverse dimension d_w. This gives the following well-known long-time scalings for $\kappa_x(t)$ [6,41]

$$\kappa_x(t) = \sigma_v^2\tau_D t\begin{cases}\left(\frac{t}{\tau_D}\right)^{1/2} & d = 2\\ \ln\left(\frac{t}{\tau_D}\right) & d = 3\\ 1 & d > 3,\end{cases} \tag{13}$$

see Appendix.

Figure 2 shows the temporal evolution of the displacement variance $\kappa_x(t)$. For times smaller than the diffusion time $\tau_D = \ell^2/d_w D$ the behavior is ballistic and $\kappa_x(t) = \sigma_v^2 t^2$. For times $t > \tau_D$, we observe the scalings (13). Note that the asymptotic scaling of the mean and the variance is not affected by the velocity distribution, but fully determined by correlation, this means by the fact that particles may return to the same channel or fiber. Here particles change velocities at constant rate τ_D^{-1}. This means particularly that low velocities do not persist and thus cannot lead to particle retention and phenomena of intermittency as observed in highly heterogeneous steady random velocity fields [7,11,53,54]. The numerical simulations employ the truncated power-law velocity distribution

$$p_v(v) = \frac{\alpha}{v_c}\left(\frac{v}{v_c}\right)^{\delta-1} \tag{14}$$

with $v < v_c$ and $\delta > 0$. The smaller δ, the higher is the probability of encountering low velocities. The mean and the variance of (14) are given by $\overline{v} = \delta v_c/(\delta+1)$ and $\sigma_v^2 = \delta v_c^2/[(\delta+2)(\delta+1)^2]$.

2. Heavy-tailed velocity distribution

If the velocity distribution is heavy tailed, this means $p_v(v) \sim v^{-1-\alpha}$ with $0 < \alpha < 2$, so is the distribution $\psi_\Delta(x)$ of space increments $\Delta x = v\tau_D$ in (8), which scales as $\psi_\Delta(x) \sim x^{-1-\alpha}$. Thus, the resulting average particle motion constitutes a Lévy flight. However, unlike in classical Lévy flights, subsequent spatial increments Δx_n are not independent due to the finite probability to return to the same velocity. Thus, we call the average particle motion here a correlated Lévy flight.

The renormalization of the particle position according to (8) renders x_{n_t} a sum of S_{n_t} independent random increments. Thus, the generalized central limit theorem implies that $c(x,t)$ given by (9) converges to a one-sided stable density for $0 < \alpha < 1$ and an extreme stable density for $1 < \alpha < 2$ [55]. This means that

$$c(x,t) = \begin{cases} g_\alpha[x/\eta(t)]/\eta(t) & 0 < \alpha < 1\\ g_\alpha[(x-\overline{v}t)/\eta(t)]/\eta(t) & 1 < \alpha < 2,\end{cases} \tag{15}$$

where we defined the scaling variable

$$\eta(t) = \gamma_{n_t} S_{n_t}^{1/\alpha}. \tag{16}$$

The function $g_\alpha(x)$ is a stable distribution of order α, which scales as $g_\alpha(x) \propto x^{-1-\alpha}$ for $x \gg 1$. The scaling variable $\eta(t)$ behaves as

$$\eta(t) = \left(\frac{t}{\tau_D}\right)^{1/\alpha}\begin{cases}\left(\frac{t}{\tau_D}\right)^{\frac{\alpha-1}{2\alpha}} & d = 2\\ \ln\left(\frac{t}{\tau_D}\right)^{\frac{\alpha-1}{\alpha}} & d = 3\\ 1 & d > 3.\end{cases} \tag{17}$$

For $0 < \alpha < 1$, the maximum of the particle distribution moves superlinearly, its velocity increases with increasing dimension. This behavior can be explained by the persistence of low velocities in $d < 4$.

Figure 3 shows the density profiles obtained from numerical simulations and the analytical scalings (15). The numerical simulations use the Pareto distribution

$$p_v(v) = \frac{\alpha}{v_c}\left(\frac{v}{v_c}\right)^{-1-\alpha}, \tag{18}$$

with $v > v_c$ and $0 < \alpha < 2$.

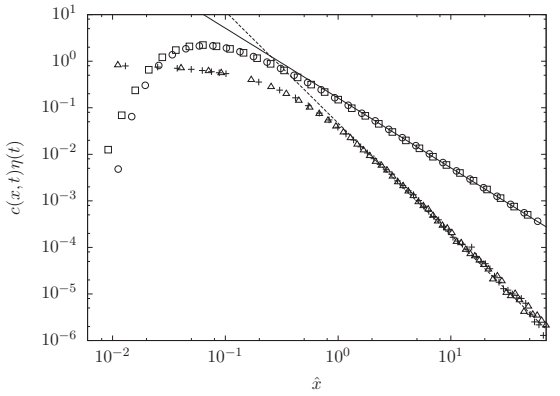

FIG. 3. Particle density for (squares and circles) $\alpha = 1/2$ and (triangles and crosses) $\alpha = 1.4$ (circles) in $d = 2$ dimensions at times $t = 20\tau_D$ and $100\tau_D$ rescaled by $\eta(t)$ versus $\hat{x} = x/\eta(t)$ for $\alpha < 1$ and $\hat{x} = (x - \overline{v}t)/\eta(t)$ for $1 < \alpha < 2$. The dashed and solid lines show the asymptotic scalings as $x^{-1-\alpha}$. The simulations use the velocity distribution (18).

B. First-passage times

We now consider the distribution of first-passage times $t(x) = \min(t|x_{n_t} \geqslant x)$ at a plane at a longitudinal position x, which is defined by

$$f(t,x) = \overline{\delta[t - t(x)]}. \tag{19}$$

In the TDRW framework employed here, $t(x) = n_x\tau_D$, where $n_x = \max(n|x_n \leqslant x)$. Note that we set the transition time $\tau = \tau_D$ for the analytical derivations. Thus, we can write $f(t,x)$ as

$$f(t,x) = \sum_{n=0}^{\infty} \overline{\delta(t - n\tau_D)\delta_{n,n_x}}. \tag{20}$$

Furthermore, mass conservation gives the following relation between $f(t,x)$ and $c(x,t)$:

$$\int_0^t dt' f(t',x) = \int_x^{\infty} dx' c(x',t). \tag{21}$$

This relationship expresses that the number of particles that have passed the position x at time t is equal to the number of particles that are to the right of the position x. It implies that

$$f(t,x) = \frac{\partial}{\partial t} \int_x^{\infty} dx' c(x',t). \tag{22}$$

The mean first-passage time $\mu_t(x)$ and its variance $\kappa_t(x)$ are defined by

$$\mu_t(x) = \int_0^{\infty} dt\, t f(t,x) = \tau_D \overline{n_x}, \tag{23}$$

$$\kappa_t(x) = \int_0^{\infty} dt [t - \mu_t(x)]^2 f(t,x) = \tau_D^2 \left(\overline{n_x^2} - \overline{n_x}^2\right). \tag{24}$$

In the following, we discuss the first-passage time distribution for velocity distributions with finite variance and heavy-tailed velocity distributions.

1. Finite velocity variance

In the case of finite velocity variance, the particle distribution $c(x,t)$ is given by (11). Thus, Eq. (22) implies for $f(t,x)$ the inverse Gaussian-type first-passage time distribution

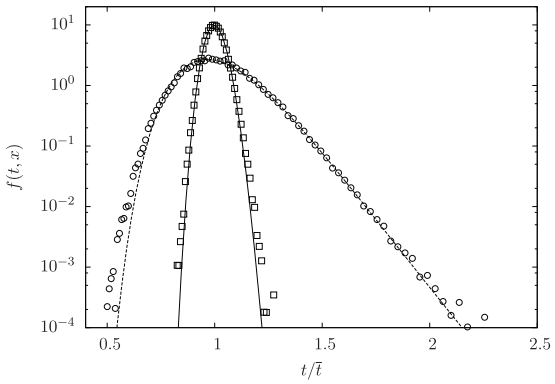

FIG. 4. First-passage time distributions for $\delta = 1/2$ (circles) and $\delta = 1.4$ (squares) in (14) for $d = 2$ dimensions at the control plane $x_c = 100\ell$ and $x_c = 5000\ell$, respectively. The dashed and the solid lines represent the analytical solution (25).

$$f(t,x) = \frac{[\kappa_x(t)\overline{v} + \mathcal{D}_x(t)(x - \overline{v}t)] \exp\left[-\frac{(x-\overline{v}t)^2}{2\kappa_x(t)}\right]}{\sqrt{2\pi\kappa_x(t)^3}}, \tag{25}$$

where the apparent dispersion coefficient $\mathcal{D}_x(t)$ is defined by

$$\mathcal{D}_x(t) = \frac{1}{2}\frac{d\kappa_x(t)}{dt}. \tag{26}$$

The mean first-passage time is given by $\mu_t(x) = x/\overline{v}$. For the variance of the first-passage time we obtain

$$\kappa_t(x) \propto \frac{\sigma_v^2\tau_D}{\overline{v}^2}\frac{x}{\overline{v}} \begin{cases} \left(\frac{x}{\overline{v}\tau_D}\right)^{1/2} & d = 2 \\ \ln\left(\frac{x}{\overline{v}\tau_D}\right) & d = 3 \\ 1 & d > 3, \end{cases} \tag{27}$$

see Appendix.

Figure 4 shows the full temporal behavior of the first-passage time distribution obtained numerical simulations for different disorder scenarios in $d = 2$ dimensions. We make use of the velocity distribution (14). We observe that the distribution of first-passage times broadens for decreasing δ because $\sigma_v^2/\overline{v}^2$ increases with decreasing δ as $1/(\delta + 2)$.

2. Heavy-tailed velocity distribution

We first consider the case $0 < \alpha < 1$. Using expression (15) in relation (22) between the first-passage time and particle distributions, we find

$$f(t,x) = \frac{x}{\eta(t)^2}\frac{d\eta(t)}{dt} F_\alpha[\eta(t)/x], \tag{28}$$

where we defined $F_\alpha(y) = g_\alpha(1/y)$; $g_\alpha(x)$ is a one-sided stable density. For $\alpha = 1/2$, $g_{1/2}(x)$ is a Lévy distribution. Thus we obtain the exact expression

$$f(t,x) = \frac{\eta(t)^{-1/2}}{x^{1/2}}\frac{d\eta(t)}{dt}\frac{a\exp[-a^2\eta(t)/2x]}{\sqrt{2\pi}}, \tag{29}$$

with a a constant. For general $0 < \alpha < 1$, $F_\alpha(y)$ behaves at large y as a stretched exponential [55,56],

$$F_\alpha(y) \sim \frac{(y\alpha)^{\frac{1-\alpha/2}{1-\alpha}} \exp\left[-c_\alpha^2(1-\alpha)(y\alpha)^{\frac{\alpha}{1-\alpha}}\right]}{\sqrt{2\pi(1-\alpha)\alpha}} \tag{30}$$

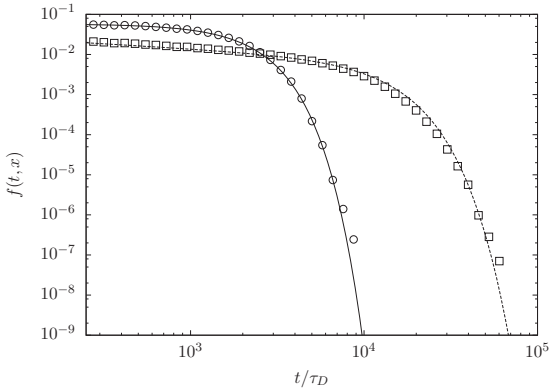

FIG. 5. First-passage time distributions at the control plane $x = 10^4$ for $\alpha = 1/2$ in $d = 2$ (squares) and $d = 3$ (circles). The solid and dashed lines represent Eq. (29) for $d = 2$ and $d = 3$ dimensions.

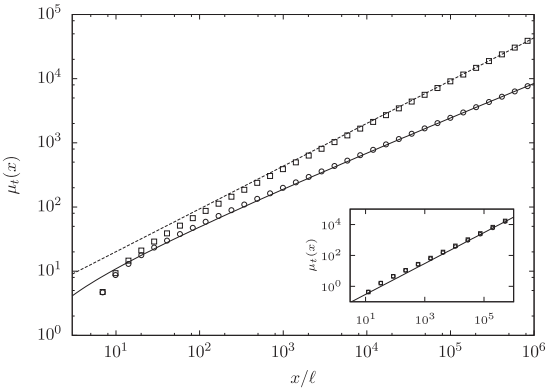

FIG. 6. Mean first-passage time for $\alpha = 1/2$ for $d = 2$ (squares) and $d = 3$ (circles). (Inset) Mean first-passage time for $\alpha = 1.4$ for $d = 2$ and $d = 3$. Lines represent the asymptotic scalings (31).

with c_α a constant that depends on the details of the heavy-tailed velocity distribution. The full behavior of $f(t,x)$ for $\alpha = 1/2$ is shown in Fig. 5 for $d < 3$ and $d = 3$ dimensions, which is in agreement with the analytical prediction (29).

The behavior of the mean first-passage time $\mu_t(x)$ with distance depends on the spatial dimension. Inserting expression (28) into (23) and using (17), we obtain the following scaling behaviors for the mean first-passage time with distance:

$$\mu_t(x) \propto \begin{cases} x^{2\alpha/(1+\alpha)} & d = 2 \\ x^\alpha \ln(x)^{1-\alpha} & d = 3 \\ x^\alpha & d > 3. \end{cases} \tag{31}$$

The mean first-passage time evolves sublinearly with distance but faster with decreasing dimension because of increasing correlation of subsequent (low) velocities. Note that the mean first-passage time is related to the harmonic mean velocity, which is dominated by low velocities. The scaling of the variance $\kappa_t(x)$ of first-passage times is obtained analogously by inserting (28) into (24) and using (17),

$$\kappa_t(x) \propto \mu_t(x)^2. \tag{32}$$

For $1 < \alpha < 2$ we use expression (15) in (22) in order to obtain

$$f(t,x) = \frac{\overline{v}\eta(t) + (x - \overline{v}t)\frac{d\eta(t)}{dt}}{\eta(t)^2} g_\alpha\left[\frac{x - \overline{v}t}{\eta(t)}\right], \tag{33}$$

where $g_\alpha(x)$ is an extreme stable density. The long-time behavior of $f(t,x)$ is obtained by noting first that $t/\eta(t)$ increases with time because $\eta(t)$ evolves sublinearly for $1 < \alpha < 2$. Thus, the asymptotic behavior of $f(t,x)$ is obtained from the behavior of $g_\alpha(x)$ for $x \to -\infty$, which is given by [55]

$$g_\alpha(x) \sim \frac{\left(\frac{|x|}{\alpha}\right)^{\frac{1-\alpha/2}{\alpha-1}} \exp\left[-c_\alpha^2(\alpha-1)\left(\frac{|x|}{\alpha}\right)^{\frac{\alpha}{\alpha-1}}\right]}{\sqrt{2\pi(1-\alpha)\alpha}}. \tag{34}$$

Thus, $f(t,x)$ behaves at long times as a stretched exponential and all first-passage time moments exist. In this case and in general for velocity distributions with $\overline{v} < \infty$, the mean first-passage time is given by $\mu_t(x) = x/\overline{v}$. The variance of the first-passage times for $1 < \alpha < 2$ scales as

$$\kappa_t(x) \propto \begin{cases} x^{(5-\alpha)/2} & d = 2 \\ x^{3-\alpha}\ln(x)^{\alpha-1} & d = 3 \\ x^{3-\alpha} & d > 3, \end{cases} \tag{35}$$

see Appendix.

The behavior of the mean first-passage time and the analytical scalings are shown in Fig. 6 for $d = 2$ and $d = 3$ dimensions for $\alpha = 1/2$ and $\alpha = 1.4$. As discussed above, for $0 < \alpha < 1$, the mean first-passage time at a control plane is larger in $d = 2$ than in $d = 3$ as a consequence of stronger persistence of low velocities.

III. RANDOM RETARDATION MODEL

We contrast the behaviors observed in the previous section to dispersion under spatially random retardation. Here particle motion is ruled by the Langevin equation

$$dx(t) = \frac{v_0 dt}{\theta[\mathbf{z}(t)]}, \quad d\mathbf{z}(t) = \sqrt{\frac{2Ddt}{\theta[\mathbf{z}(t)]}}\boldsymbol{\zeta}(t), \tag{36}$$

where the retardation factor $\theta(\mathbf{z})$ is distributed according to $p_\theta(\theta)$. Note that unlike in the Matheron–de Marsily model, disorder here acts also on diffusion in the transverse directions, which affects disorder sampling. We define the operational time through $dt(s) = \theta[\mathbf{z}(s)]ds$ and transform $t \to s$ in (36) to obtain

$$dx(s) = v_0 ds, \quad d\mathbf{z}(s) = \sqrt{2Dds}\boldsymbol{\zeta}(s). \tag{37}$$

This subordinated process describes a biased Brownian motion. In order to determine the large-scale particle motion, we coarse grain (37) so that each step corresponds to a change in θ, which occurs whenever a particle diffuses to a contiguous channel; this means for $\|\Delta\mathbf{z}(s)\| = \ell$. The (operational) time σ needed for this transition is given by the diffusive first-passage time, which is exponentially distributed with mean τ_D. Diffusion depends on the local retardation coefficient. Therefore, the coarse-grained equations read as

$$x_{n+1} = x_n + v_0\sigma_n \quad t_{n+1} = t_n + \theta_n\sigma_n, \tag{38}$$

where we set $\theta_n \equiv \theta(\mathbf{z}_n)$. The numerical simulations reported in the following are based on this TDRW. For the derivations of the average dispersion behavior, in the following, we approximate the operational time σ_n needed for single step by its mean τ_D. Thus, the transition length for a single step in this approximation is constant and equal to $\Delta x = v_0\tau_D$. The transition time is $\tau = \theta\tau_D$, which is distributed according to

$$\psi(t) = \frac{1}{\tau_D} p_\theta(t/\tau_D). \tag{39}$$

As above, transverse particle motion describes a random walk on a d_w-dimensional hyperlattice, and, as a consequence, the $\{\theta_n\}$ and thus the transition times $\{\tau_n\}$ form correlated random series. Unlike in the Matheron–de Marsily model, here the disorder affects the temporal increments. The particle time t_n can be renormalized into families of independent increments as

$$t_n = \gamma_n \sum_{i=1}^{S_n} \theta_i \tau_D. \tag{40}$$

Note the duality of the particle motions given by (6)–(8) in the Matheron–de Marsily model and (38)–(40) here.

A. First-passage times

The first-passage time distribution here is given by

$$f(t,x) = \sum_{n=0}^{\infty} \overline{\delta(t - t_{n_x})}, \tag{41}$$

where $n_x = x/(v_0\tau_D)$. The particle time t_{n_x} is according to (40) the sum of independent random variables. Note the duality with expression (9) for the particle density in the Matheron–de Marsily model.

1. Finite disorder variance

We first consider the case of finite disorder variance. Exploiting the duality between (41) and (9), we obtain from (11) that $f(t,x)$ follows at large $x \gg v_0\tau_D$ the Gaussian distribution

$$f(t,x) = \frac{\exp\left[-\frac{(t-x\overline{\theta}/v_0)^2}{2\kappa_t(x)}\right]}{\sqrt{2\pi\kappa_x(t)}}, \tag{42}$$

where the mean first-passage time is $x\overline{\theta}/v_0$ and the variance of the first-passage time is

$$\kappa_t(x) = \sigma_\theta^2 \tau_D \frac{x}{v_0} \begin{cases} \left(\frac{x}{v_0\tau_D}\right)^{1/2} & d = 2 \\ \ln\left(\frac{x}{v_0\tau_D}\right) & d = 3 \\ 1 & d > 3. \end{cases} \tag{43}$$

For dimensions $d < 4$, the variance of the first-passage time scales superdiffusively with distance.

2. Heavy-tailed disorder distribution

We now consider heavy-tailed distributions of the retardation coefficient which for $\theta \gg 1$ behave as $p_\theta(\theta) \sim \theta^{-1-\beta}$ with $0 < \beta < 2$. The generalized central limit theorem indicates that the first-passage time distribution converges towards a stable law for $S_n \gg 1$ because (40) is the sum of independent increments. Thus, we obtain in analogy to the particle distributions (15) in the random velocity model

$$f(t,x) = \begin{cases} g_\beta[t/\hat{\eta}(x)]/\hat{\eta}(x) & 0 < \beta < 1 \\ g_\beta[(t - x\overline{\theta}/v)/\hat{\eta}(x)]/\hat{\eta}(x) & 1 < \beta < 2. \end{cases} \tag{44}$$

For $0 < \beta < 1$, $g_\beta(t)$ is a one-sided stable density, and for $1 < \beta < 2$ it is an extreme stable density [55]. The scaling functions behaves as $g_\beta(t) \propto t^{-1-\beta}$ at times $t \gg \tau_D$. The scaling variable $\hat{\eta}(x)$ is given by $\hat{\eta}(x) = \eta[x/(v_0\tau_D)]$, where $\eta(t)$ is defined by (16).

The power-law tailing is not affected by the correlation of transition times, which impacts, however, the scaling of the maximum $f_m(x)$ of the first-passage time distribution according to $f_m(x) \propto 1/\hat{\eta}(x)$. For $\alpha < 1$ the time $\tau_m(x)$ of maximum arrival scales as $\tau_m(x) \propto \hat{\eta}(x)$. This is illustrated in Fig. 7, which compares the first-passage time distributions obtained from numerical random walk simulations with the derived scalings. Note that Fig. 7 corresponds to Fig. 3 for the particle distribution.

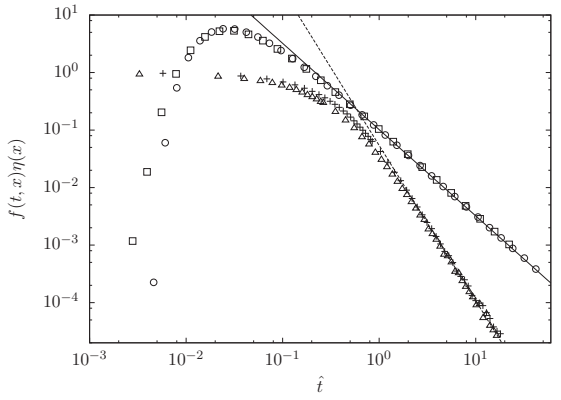

FIG. 7. First-passage time distributions for $\beta = 1/2$ (circles and squares) and $\beta = 1.7$ (triangles and crosses) in $d = 3$ dimensions at the control plane $x_c = 10^2\ell$ and $5 \times 10^2\ell$ rescaled by $\eta(x)$ versus $\hat{t} = t/\eta(x)$ for $\beta < 1$ and $\hat{t} = (t - \overline{\theta}x/v)/\eta(x)$ for $1 < \beta < 2$. The dashed and solid lines represent the scaling $t^{-1-\beta}$ for $\beta = 1/2$ and $\beta = 1.7$, respectively.

The numerical time-domain random walk simulations are performed using the following Pareto distribution for the retardation coefficient θ

$$p_\theta(\theta) = \frac{\beta}{\theta_0}\left(\frac{\theta}{\theta_0}\right)^{-1-\beta} \tag{45}$$

with $\theta > \theta_0$.

B. Spatial density and moments

The average particle density is given by

$$c(\mathbf{x},t) = \sum_{n=0}^{\infty} \overline{\langle \delta(x - x_n)\delta(\mathbf{z} - \mathbf{z}_n)\delta_{n,n_t}\rangle}. \tag{46}$$

Transverse particle motion is equivalent to an unbiased random walk in the presence of quenched random traps [1,34]. Thus, the mean displacement in transverse direction is $\overline{\mathbf{z}(t)} = \mathbf{0}$ and the mean squared displacement is $\kappa_z(t) = \overline{\mathbf{z}(t)^2} = \ell^2\overline{n_t}$. The longitudinal particle position is here given by $x(t) = n_t v_0\tau_D$. Note that we set the operational time $\sigma = \tau_D$ for the analytical

derivations. Thus, the particle density is

$$c(x,t) = \sum_{n=0}^{\infty} \overline{\delta(x - n v_0 \tau_D)\delta_{n,n_t}}, \tag{47}$$

which is of the same form as the first-passage time distribution (20) in the Matheron–de Marsily model. Thus, in analogy with (22), mass conservation gives the following relation between the first-passage time distribution and the particle distribution:

$$c(x,t) = \frac{\partial}{\partial x} \int_t^{\infty} dt' f(t',x). \tag{48}$$

The mean displacement and the displacement variance are given by

$$\mu_x(t) = \int dx x c(x,t) = v_0 \tau_D \overline{n_t}, \tag{49}$$

$$\kappa_x(t) = \int dx [x - \mu_x(t)]^2 c(x,t) = v_0^2 \tau_D^2 \left(\overline{n_t^2} - \overline{n_t}^2\right). \tag{50}$$

Note that the mean displacement in longitudinal direction is proportional to the transverse mean squared displacement $\mu_x(t) \propto \kappa_z(t)$.

1. Finite disorder variance

For $\overline{\theta^2} < \infty$, the transverse mean squared displacement evolves diffusively as $\kappa_z(t) = 2d_w Dt/\overline{\theta}$ [34], this means transverse disorder sampling is effectively diffusive as for the Matheron–de Marsily model. As a result, the longitudinal mean displacement evolves linearly with time as $\mu_x(t) = v_0 t/\overline{\theta}$, and the displacement variance behaves as

$$\kappa_x(t) \propto v_0^2 \tau_D \frac{\sigma_\theta^2}{\overline{\theta}^2} \frac{t}{\overline{\theta}} \begin{cases} \left(\frac{t}{\overline{\theta}\tau_D}\right)^{1/2} & d = 2 \\ \ln\left(\frac{t}{\overline{\theta}\tau_D}\right) & d = 3 \\ 1 & d > 3, \end{cases} \tag{51}$$

see Appendix. These expressions correspond to (27) for the moments of the first-passage time in the Matheron–de Marsily model. Using the duality between the Matheron–de Marsily model and the random retardation model, we see immediately from (25) that the spatial particle distribution is given by

$$c(x,t) = \frac{\left[\kappa_t(x)\frac{\overline{\theta}}{v_0} + \mathcal{D}_t(x)\left(t - \frac{x\overline{\theta}}{v_0}\right)\right]}{\sqrt{2\pi\kappa_t(x)^3}} \times \exp\left[-\frac{\left(t - \frac{x\overline{\theta}}{v_0}\right)^2}{2\kappa_t(x)}\right], \tag{52}$$

where $2\mathcal{D}_t(x) = d\kappa_t(x)/dx$.

2. Heavy-tailed disorder distribution

Transverse particle motion here is subdiffusive [34], which affects the efficiency of disorder sampling across strata or channels, which in turn affects the longitudinal particle motion. For $0 < \beta < 1$, we obtain from (48) in analogy with (28)

$$c(x,t) = \frac{t}{\hat{\eta}(x)^2} \frac{d\hat{\eta}(x)}{dx} F_\beta[\hat{\eta}(x)/t], \tag{53}$$

where $F_\beta(y) = g_\beta(1/y)$. It behaves at large y as the stretched exponential (29). Along the same lines, we obtain for

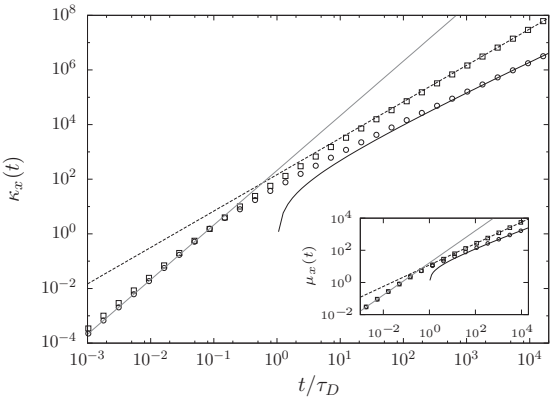

FIG. 8. Longitudinal variance of particle displacements for $\beta = 1/2$ and for $d = 2$ (squares) and $d = 3$ (circles). Black lines are analytical scalings, the gray line is ballistic. (Inset) Mean position, black lines denote the analytical scalings, the gray line linear scaling.

$1 < \beta < 2$

$$c(x,t) = \frac{\frac{\overline{\theta}\hat{\eta}(x)}{v_0} + \left(t - \frac{x\overline{\theta}}{v_0}\right)\frac{d\hat{\eta}(x)}{dx}}{\hat{\eta}(x)^2} g_\beta\left[\frac{t - \frac{x\overline{\theta}}{v_0}}{\eta(t)}\right], \tag{54}$$

with $g_\beta(x)$ an extreme stable density. The behavior of $c(x,t)$ at large distances corresponds to the behavior of $g_\beta(x)$ as $x \to -\infty$, which is given by the stretched exponential (34).

For $d \leqslant 3$ dimensions, particle motion is CTRW-like, characterized by correlation in subsequent time increments, which is quantified by the renormalization of the particle time according to (40) and encoded in (53) and (54) by $\hat{\eta}(x)$. For $0 < \beta < 1$, we obtain by inserting the scaling form (53) into definitions (49) and (50) for the displacement mean and variance the quasiballistic scaling behaviors

$$\kappa_x(t) \propto \mu_x(t)^2 \propto \begin{cases} t^{4\beta/(1+\beta)} & d = 2 \\ t^{2\beta} \ln(t)^{2-2\beta} & d = 3. \end{cases} \tag{55}$$

This behavior is caused by the long residence times in individual channels or strata, which on one hand slows the mean displacement down and on the other hand leads to the quasiballistic scaling.

For $1 < \beta < 2$, the retardation in individual channels is weaker and the mean displacement is given by $\mu_x(t) \propto v_0 t/\overline{\theta}$ for all dimensions, while the variance scales as

$$\kappa_x(t) \propto \begin{cases} t^{(5-\beta)/2} & d = 2 \\ t^{3-\beta} \ln(t)^{\beta-1} & d = 3, \end{cases} \tag{56}$$

see Appendix. While dispersion in the absence of diffusion is ballistic, the observed behaviors here are entirely due to the diffusive disorder sampling across channels of equal retardation properties. Particle motion is only CTRW-like because the quenched nature of the underlying disorder is inherited through the correlation of subsequent θ_n.

For $d > 3$, particles describe a CTRW in longitudinal direction because of the efficient diffusive transverse sampling through which the disorder experienced by the particles assumes an annealed character. Thus, displacement mean and variance show the scaling known from uncorrelated CTRW

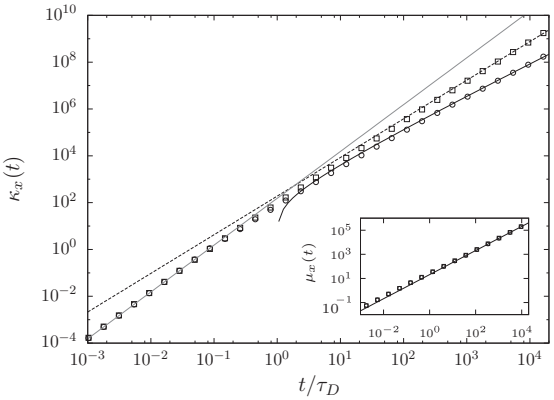

FIG. 9. Longitudinal variance of particle displacements for $\beta = 1.7$ and for $d = 2$ (squares) and $d = 3$ (circles). Black lines are analytical scalings; the gray line is ballistic. (Inset) Mean position, the gray line denotes linear scaling.

[57,58], this means

$$\mu_x(t) \propto t^{\beta} \quad \kappa_x(t) \propto t^{2\beta} \tag{57}$$

for $0 < \beta < 1$ and

$$\mu_x(t) \propto t \quad \kappa_x(t) \propto t^{3-\beta} \tag{58}$$

for $1 < \beta < 2$.

Figures 8 and 9 show the temporal evolution of the mean and the variance of particle displacements in $d = 2$ and $d = 3$ dimensions for power-law distributed retardation coefficients with exponents $\beta = 1/2$ and $\beta = 1.7$, respectively. We observe ballistic behavior at times shorter than τ_D, which is the characteristic time for the onset of transverse disorder sampling. For times larger than τ_D, the moments evolve towards their respective asymptotic scalings, which depend on the heterogeneity and the dimensionality of the medium.

IV. CONCLUSIONS

In conclusion we have analyzed the impact of diffusion on anomalous transport in stratified and fibrous disordered media for which transport is otherwise ballistic. We have shown how diffusive disorder sampling changes the nature of average transport depending on the microscopic transport mechanisms, disorder distribution, and dimensionality of space. Transverse diffusion acts differently on longitudinal transport properties and on the first-passage time distributions depending on the disorder model. There is complete duality in spatial and temporal features between the random velocity model and the random retardation model. The quenched nature of the underlying disorder is inherited by the average particle motion in $d \leqslant 3$ dimensions, for which we discover correlated Lévy flights in the case of the Matheron–de Marsily model with heavy-tailed velocities and correlated biased continuous time random walks for the random retardation model with heavy-tailed retardation distribution. For $d > 4$ the disorder particles experience assumes an annealed character, which leads to Lévy flight dynamics in the random velocity and biased CTRW behavior in the random retardation model. These results shed light on the pivotal role of diffusion for the prediction and interpretation of anomalous transport behaviors and signal transmission in disordered structures.

ACKNOWLEDGMENTS

The research leading to these results has received funding from the European Research Council under the European Union's Seventh Framework Programme (FP7/2007-2013)/ ERC Grant Agreement No. 617511 (MHetScale).

APPENDIX: MEAN AND VARIANCE OF DISPLACEMENT AND FIRST-PASSAGE TIME

Here we derive the asymptotic scalings of the moments of the first-passage time distribution for the Matheron–de Marsily model with the velocity distribution (18) and the displacement moments for the random retardation model with the distribution (45) of the retardation coefficient. As we discuss in the main text, the random velocity model and the random retardation model are dual. The first-passage time distribution (20) of the Matheron–de Marsily model corresponds to the particle distribution (47) in the random retardation model. The first-passage time in the random velocity model is given by

$$t(x) = n_x \tau_D \tag{A1}$$

and the position in the random retardation model by

$$x(t) = n_t v_0 \tau_D. \tag{A2}$$

Thus, mean and variance of first-passage time and displacement can be written as

$$\mu_\theta(\xi) = \theta_0 \overline{n_\xi} \quad \kappa_\theta(x) = \theta_0^2 \left(\overline{n_\xi^2} - \overline{n_\xi}^2\right), \tag{A3}$$

where $\xi = t$, $\theta = x$, and $\theta_0 = v_0 \tau_D$ for the displacement moments and $\xi = x$ and $\theta = t$ and $\theta_0 = \tau_D$ for the first-passage time moments. Note that the asymptotic scalings depend only on the moments of the renewal process n_ξ. The derivation of the behavior of the moments of n_ξ can be found in Ref. [34] for the power-law distribution $\psi_\xi \sim (\xi/\xi_0)^{-1-\nu}$ with $0 < \nu < 2$. Note that $\nu = \alpha$ for the random velocity and $\nu = \beta$ for the random retardation model. For the convenience of the reader, in the following, we provide the derivation for the case of $1 < \nu < 2$.

The distribution of n_ξ is given by

$$p_n(\xi) = \overline{\delta_{n,n_\xi}}. \tag{A4}$$

Its ith moments are defined by

$$h_k(\xi) = \sum_{n=0}^{\infty} n^k p_n(\xi). \tag{A5}$$

The Laplace transform of (A4) can be written for large n as [34]

$$p_n^*(\lambda) = -\frac{1}{\lambda} \frac{d}{dn} f_n^*(\lambda), \tag{A6}$$

where we defined

$$f_n^*(\lambda) = \psi^*(\gamma_n \lambda)^{S_n}. \tag{A7}$$

Likewise, we write the Laplace transform of the moments (A5) as

$$h_k^*(\lambda) = -\frac{1}{\lambda} \int_0^{\infty} dn n^k \frac{d}{dn} f_n^*(\lambda), \tag{A8}$$

for which we obtain by integration by parts

$$h_k^*(\lambda) = \frac{1}{\lambda} k \int_0^\infty dn n^{k-1} f_n^*(\lambda). \tag{A9}$$

As outlined above, we consider the case $\psi_\xi(\xi) \propto (\xi/\xi_0)^{-1-\nu}$ and focus on the case $1 < \nu < 2$. The Laplace transform of $\psi_\xi(\xi)$ is for $\lambda\xi_0 \ll 1$ given by

$$\psi_\xi^*(\lambda) = 1 - \bar{\xi}\lambda + a_\nu \lambda^\nu, \tag{A10}$$

where the constant a_ν depends on the specific form of the distribution $\psi_\xi(\xi)$. For $\nu > 2$, we set $\nu = 2$ in (A10) and a_ν is equal to $\overline{\xi^2}/2$. Using this expansion, we can write (A7) as

$$f_n^*(\lambda) = \exp\left[S_n \ln\left(1 - \bar{\xi}\gamma_n\lambda + a_\nu \gamma_n^\nu \lambda^\nu\right)\right]. \tag{A11}$$

Expansion of the exponent gives

$$f_n^*(\lambda) = \exp\left(-\bar{\xi} S_n \gamma_n \lambda + A_\nu S_n \gamma_n^\nu \lambda^\nu\right), \tag{A12}$$

where $A_\nu = a_\nu$ for $1 < \nu < 2$ and $A_\nu = \sigma_\xi^2/2$ for $\nu > 2$ with $\sigma_\xi^2 = \overline{\xi^2} - \bar{\xi}^2$. Further expanding the exponential, we obtain in leading order

$$f_n^*(\lambda) \approx \exp(-n\bar{\xi}\lambda)\left(1 + S_n^{1-\nu} n^\nu A_\nu \lambda^\nu\right), \tag{A13}$$

where we used that $\gamma_n = n/S_n$.

For $d = 2$, this means $d_w = 1$, we obtain for the moments

$$h_k^*(\lambda) = \frac{1}{\lambda} k \int_0^\infty dn n^{k-1} \exp(-n\bar{\xi}\lambda) + \frac{1}{\lambda} k \int_0^\infty dn n^{k+\frac{\nu-1}{2}} A_\nu \lambda^\nu \exp(-n\bar{\xi}\lambda). \tag{A14}$$

Scaling of $n \to n\bar{\xi}\lambda$ gives

$$h_k^*(\lambda) = \frac{\lambda^{-1-k}}{\bar{\xi}^k} k\Gamma(k) + \frac{1}{\lambda}(\lambda\bar{\xi})^{-k-\frac{1-\nu}{2}} A_\nu k\Gamma[1 + k + (\nu - 1)/2]. \tag{A15}$$

Inverse Laplace transform gives

$$h_k(\xi) = (\xi/\bar{\xi})^k + B_{2k}(\xi/\bar{\xi})^{k-\frac{\nu-1}{2}}, \tag{A16}$$

with

$$B_{2k} = \frac{A_\nu}{\bar{\xi}^\nu} \frac{k\Gamma[1 + k + (\nu - 1)/2]}{\Gamma[1 + k - (\nu - 1)/2]}. \tag{A17}$$

Specifically, we obtain for the mean and variance of n_ξ in leading order

$$\overline{n_\xi} = \xi/\bar{\xi}, \tag{A18}$$

$$\overline{n_\xi^2} - \overline{n_\xi}^2 \propto \frac{A_\nu}{\bar{\xi}^\nu}(\xi/\bar{\xi})^{2-\frac{\nu-1}{2}}. \tag{A19}$$

For $d = 3$, this means $d_w = 2$, we derive along the same lines that

$$h_k(\xi) = (\xi/\bar{\xi})^k + B_{3k}(\xi/\bar{\xi})^{1+k-\nu} \ln(\xi/\bar{\xi})^{\nu-1}, \tag{A20}$$

with $B_{3k} \propto A_\nu/\bar{\xi}^\nu$ a constant. Mean and variance of n_ξ are given by

$$\overline{n_\xi} = \xi/\bar{\xi}, \tag{A21}$$

$$\overline{n_\xi^2} - \overline{n_\xi}^2 \propto \frac{A_\nu}{\bar{\xi}^\nu}(\xi/\bar{\xi})^{3-\nu} \ln(\xi/\bar{\xi})^{\nu-1}. \tag{A22}$$

For $d > 3$, this means $d_w > 2$, we find

$$h_k(\xi) = (\xi/\bar{\xi})^k + B_{4k}(\xi/\bar{\xi})^{1+k-\nu}, \tag{A23}$$

with $B_{4k} = A_\nu/\bar{\xi}^\nu$ a constant. Thus, we obtain for the mean and variance of n_ξ

$$\overline{n_\xi} = \xi/\bar{\xi}, \tag{A24}$$

$$\overline{n_\xi^2} - \overline{n_\xi}^2 \propto \frac{A_\nu}{\bar{\xi}^\nu}(\xi/\bar{\xi})^{3-\nu}. \tag{A25}$$

[1] J. P. Bouchaud and A. Georges, Phys. Rep. **195**, 127 (1990).
[2] J. Szymanski and M. Weiss, Phys. Rev. Lett. **103**, 038102 (2009).
[3] M. Dentz and D. Bolster, Phys. Rev. Lett. **105**, 244301 (2010).
[4] I. M. Sokolov, Soft Matter **8**, 9043 (2012).
[5] H. Scher and M. Lax, Phys. Rev. B **7**, 4491 (1973).
[6] M. Matheron and G. de Marsily, Water Resour. Res. **16**, 901 (1980).
[7] B. Berkowitz and H. Scher, Phys. Rev. Lett. **79**, 4038 (1997).
[8] J. H. Cushman and T. R. Ginn, Water Resour. Res. **36**, 3763 (2000).
[9] J. D. Seymour, J. P. Gage, S. L. Codd, and R. Gerlach, Phys. Rev. Lett. **93**, 198103 (2004).
[10] B. Berkowitz, A. Cortis, M. Dentz, and H. Scher, Rev. Geophys. **44**, RG2003 (2006).
[11] T. Le Borgne, M. Dentz, and J. Carrera, Phys. Rev. Lett. **101**, 090601 (2008).
[12] B. Bijeljic, P. Mostaghimi, and M. J. Blunt, Phys. Rev. Lett. **107**, 204502 (2011).
[13] M. Holzner, V. L. Morales, M. Willmann, and M. Dentz, Phys. Rev. E **92**, 013015 (2015).
[14] A. Caspi, R. Granek, and M. Elbaum, Phys. Rev. Lett. **85**, 5655 (2000).
[15] K. R. Swanson, C. Bridge, J. Murray, and E. C. Alvord, J. Neurol. Sci. **216**, 1 (2003).
[16] E. Barkai, Y. Garini, and R. Metzler, Phys. Today **65**, 29 (2012).
[17] C. Manzo, J. A. Torreno-Pina, P. Massignan, G. J. Lapeyre, Jr., M. Lewenstein, and M. F. García Parajo, Phys. Rev. X **5**, 011021 (2015).
[18] P. Barthelemy, J. Bertolotti, and D. S. Wiersma, Nature **453**, 495 (2008).
[19] P. Barthelemy, J. Bertolotti, K. Vynck, S. Lepri, and D. S. Wiersma, Phys. Rev. E **82**, 011101 (2010).

[20] M. F. Shlesinger, B. J. West, and J. Klafter, Phys. Rev. Lett. **58**, 1100 (1987).
[21] J. Klafter and I. Sokolov, Phys. World **18**, 29 (2005).
[22] D. A. Benson, S. W. Wheatcraft, and M. M. Meerschaert, Water Resour. Res. **36**, 1403 (2000).
[23] D. Brockmann and T. Geisel, Phys. Rev. Lett. **90**, 170601 (2003).
[24] V. Zaburdaev, S. Denisov, and J. Klafter, Rev. Mod. Phys. **87**, 483 (2015).
[25] R. Metzler and J. Klafter, Phys. Rep. **339**, 1 (2000).
[26] R. Metzler and J. Klafter, J. Phys. A: Math. Gen. **37**, R161 (2004).
[27] J. H. Cushman, X. Hu, and T. R. Ginn, J. Stat. Phys. **75**, 859 (1994).
[28] S. C. Kou and X. Sunney Xie, Phys. Rev. Lett. **93**, 180603 (2004).
[29] M. Magdziarz, A. Weron, K. Burnecki, and J. Klafter, Phys. Rev. Lett. **103**, 180602 (2009).
[30] J. H. Cushman, D. O'Malley, and M. Park, Phys. Rev. E **79**, 032101 (2009).
[31] T. Miyaguchi and T. Akimoto, Phys. Rev. E **83**, 031926 (2011).
[32] M. Dentz, A. Russian, and P. Gouze, Phys. Rev. E **93**, 010101 (2016).
[33] T. Akimoto, E. Barkai, and K. Saito, Phys. Rev. Lett. **117**, 180602 (2016).
[34] A. Russian, M. Dentz, and P. Gouze, Phys. Rev. E **96**, 022156 (2017).
[35] M. Dentz and A. Castro, Geophys. Res. Lett. **36**, L03403 (2009).
[36] P. K. Kang, M. Dentz, T. Le Borgne, and R. Juanes, Phys. Rev. Lett. **107**, 180602 (2011).
[37] V. Cvetkovic, A. Fiori, and G. Dagan, Water Resour. Res. **50**, 5759 (2014).
[38] A. Tyukhova, M. Dentz, W. Kinzelbach, and M. Willmann, Phys. Rev. Fluids **1**, 074002 (2016).
[39] A. Comolli and M. Dentz, Eur. Phys. J. B **90**, 166 (2017).
[40] J. P. Bouchaud, A. Georges, J. Koplik, A. Provata, and S. Redner, Phys. Rev. Lett. **64**, 2503 (1990).
[41] G. Zumofen, J. Klafter, and A. Blumen, J. Stat. Phys. **65**, 991 (1991).
[42] M. Dentz, T. Le Borgne, and J. Carrera, Phys. Rev. E **77**, 020101 (2008).
[43] G. Dagan and E. Bressler, Soil Sci. Soc. Am. J. **43**, 461 (1979).
[44] T. R. Ginn, C. S. Simmons, and B. D. Wood, Water Resour. Res. **31**, 2689 (1995).
[45] O. A. Cirpka and P. K. Kitanidis, Water Resour. Res. **36**, 1209 (2000).
[46] J. Bear, *Dynamics of Fluids in Porous Media* (American Elsevier, New York, 1972).
[47] F. Delay, G. Porel, and P. Sardini, Compt. Rend. Geosci. **334**, 967 (2002).
[48] M. Dentz, P. Gouze, A. Russian, J. Dweik, and F. Delay, Adv. Wat. Res. **49**, 13 (2012).
[49] F. Delay, P. Ackerer, and C. Danquigny, Vadose Zone J. **4**, 360 (2005).
[50] S. L. Painter, V. Cvetkovic, and O. Pensado, Nucl. Technol. **163**, 129 (2008).
[51] B. Noetinger, D. Roubinet, A. Russian, T. Le Borgne, F. Delay, M. Dentz, J.-R. De Dreuzy, and P. Gouze, Transp. Porous Media **115**, 345 (2016).
[52] G. H. Vineyard, J. Math. Phys. **4**, 1191 (1963).
[53] A. Fiori, I. Jankovic, G. Dagan, and V. Cvetkovic, Water Resour. Res. **43**, W09407 (2007).
[54] M. Dentz, P. K. Kang, A. Comolli, T. Le Borgne, and D. R. Lester, Phys. Rev. Fluids **1**, 074004 (2016).
[55] V. V. Uchaikin and V. M. Zolotarev, *Chance and Stability: Stable Distributions and Their Applications* (Walter de Gruyter, Utrecht, 1999).
[56] T. Koren, M. A. Lomholt, A. V. Chechkin, J. Klafter, and R. Metzler, Phys. Rev. Lett. **99**, 160602 (2007).
[57] M. Shlesinger, J. Stat. Phys. **10**, 421 (1974).
[58] G. Margolin and B. Berkowitz, Phys. Rev. E **65**, 031101 (2002).